SANDIA REPORT
SAND2018-10877
Unlimited Release
Printed September 2018

Engineering Spin-Orbit Interaction in Silicon

Tzu-Ming Lu, Leon Maurer, Ezra Bussmann, Charles T. Harris, Lisa A. Tracy, and Keshab Sapkota

Prepared by
Sandia National Laboratories
Albuquerque, New Mexico 87185 and Livermore, California 94550

Sandia National Laboratories is a multimission laboratory managed and operated by National Technology and Engineering Solutions of Sandia, LLC, a wholly owned subsidiary of Honeywell International, Inc., for the U.S. Department of Energy's National Nuclear Security Administration under contract DE-NA0003525.

Sandia National Laboratories

Issued by Sandia National Laboratories, operated for the United States Department of Energy by National Technology and Engineering Solutions of Sandia, LLC.

Available to DOE and DOE contractors from

U.S. Department of Energy
Office of Scientific and Technical Information
P.O. Box 62
Oak Ridge, TN 37831

Telephone: (865) 576-8401
Facsimile: (865) 576-5728
E-Mail: reports@osti.gov
Online ordering: http://www.osti.gov/scitech

Available to the public from

U.S. Department of Commerce
National Technical Information Service
5301 Shawnee Rd
Alexandria, VA 22312

Telephone: (800) 553-6847
Facsimile: (703) 605-6900
E-Mail: orders@ntis.gov
Online order: https://classic.ntis.gov/help/order-methods/

SAND2018-10877
Printed September 2018
Unlimited Release

Engineering Spin-Orbit Interaction in Silicon

Tzu-Ming Lu
Department of Quantum Phenomena
Sandia National Laboratories
P. O. Box 5800
Albuquerque, New Mexico 87185-MS1314

Leon Maurer
Department of Non-Conventional Computing Tech
Sandia National Laboratories
P. O. Box 5800
Albuquerque, New Mexico 87185-MS1322

Ezra Bussmann
Department of Fab Tech Development
Sandia National Laboratories
P. O. Box 5800
Albuquerque, New Mexico 87185-MS1304

Charles T. Harris
Department of Nanosystems Synthesis/Analysis
Sandia National Laboratories
P. O. Box 5800
Albuquerque, New Mexico 87185-MS1304

Lisa A. Tracy
Department of Quantum Phenomena
Sandia National Laboratories
P. O. Box 5800
Albuquerque, New Mexico 87185-MS1303

Keshab Sapkota
Department of Advanced Materials Sciences
Sandia National Laboratories
P. O. Box 5800
Albuquerque, New Mexico 87185-MS1086

Abstract

There has been much interest in leveraging the topological order of materials for quantum information processing. Among the various solid-state systems, one-dimensional topological superconductors made out of strongly spin-orbit-coupled nanowires have been shown to be the most promising material platform. In this project, we investigated the feasibility of turning silicon, which is a non-topological semiconductor and has weak spin-orbit coupling, into a one-dimensional topological superconductor. Our theoretical analysis showed that it is indeed possible to create a sizable effective spin-orbit gap in the energy spectrum of a ballistic one-dimensional electron channel in silicon with the help of nano-magnet arrays. Experimentally, we developed magnetic materials needed for fabricating such nano-magnets, characterized the magnetic behavior at low temperatures, and successfully demonstrated the required magnetization configuration for opening the spin-orbit gap. Our results pave the way toward a practical topological quantum computing platform using silicon, one of the most technologically mature electronic materials.

ACKNOWLEDGMENTS

We thank John Gamble at Microsoft Corporation for his technical advice during the proposal stage and the first half of the project execution period. Measurements of magnetic moments of magnetic thin films were performed by Serena Eley at Los Alamos National Laboratory. Low-temperature transport experiments and programming of nano-magnets were carried out in Mike Lilly's labs at the Center for Integrated NanoTechnologies (CINT). Assistance in materials development and device fabrication from John Nogan and Willard Ross in the CINT Integration Lab is much appreciated. Illuminating discussions with Jeff Nelson (Sandia), Art Fischer (Sandia), Rick Muller (Sandia), Carlos Gutierrez (Sandia), Wolfgang Porod (University of Notre Dame), Gary Bernstein (University of Notre Dame), Michel Pioro-Ladrière (Université de Sherbrooke), and Javad Shabani (New York University) facilitated the program development and helped accelerating the progress of this project.

This work was supported by the Laboratory Directed Research and Development Program at Sandia National Laboratories as project number 200238 and was performed, in part, at the Center for Integrated Nanotechnologies, an Office of Science User Facility operated for the U.S. Department of Energy (DOE) Office of Science. The views expressed in the article do not necessarily represent the views of the U.S. Department of Energy or the United States Government.

TABLE OF CONTENTS

FIGURES

TABLES

NOMENCLATURE

Abbreviation	Definition
1D	One-dimensional
2D	Two-dimensional
3D	Three-dimensional
EBL	Electron beam lithography
FET	Field-effect transistor
HCP	Hexagonal close packed
HFET	Heterostructure field-effect transistor
HSQ	hydrogen silsesquioxane
ICP	Inductively coupled plasma
IPA	isopropyl alcohol
LDRD	Laboratory Directed Research and Development
MFM	Magnetic force microscopy
MFP	Mean free path
MIBK	methyl isobutyl ketone
MOS	metal-oxide-semiconductor
MZM	Majorana zero mode
PMMA	poly-methyl methacrylate
RE	Rare earth
RIE	Reactive ion etching
SEM	scanning electron microscope
SOC	Spin-orbit coupling
TEM	Transmission electron microscopy
TM	Transition metal
XRD	X-ray diffraction

1. INTRODUCTION

In recent years, much progress has been made toward realizing quantum computation along many fronts. The most promising approaches are solid-state systems, including the superconducting and semiconductor qubit platforms [1-4]. In these solid-state systems, however, electrical and magnetic noise often causes information to be lost through interactions between the qubits and the environment. This information loss behavior can be characterized by a phase coherence time, T_2. Quantum operations in solid-state systems are often limited by very short T_2, which makes read-out and scaling very challenging tasks.

A potential workaround is to encode information in the topological order of materials [5]. In this case, the non-local nature of the wave functions protects the information from being destroyed by local noise and potentially provides a much more robust quantum computation platform than non-topological systems. One class of topological excitations that exhibit the required non-Abelian statistics for topological qubits are the Majorana zero modes (MZMs). These modes are predicted to emerge at the interface between a topological superconductor and a topologically trivial material [6-7].

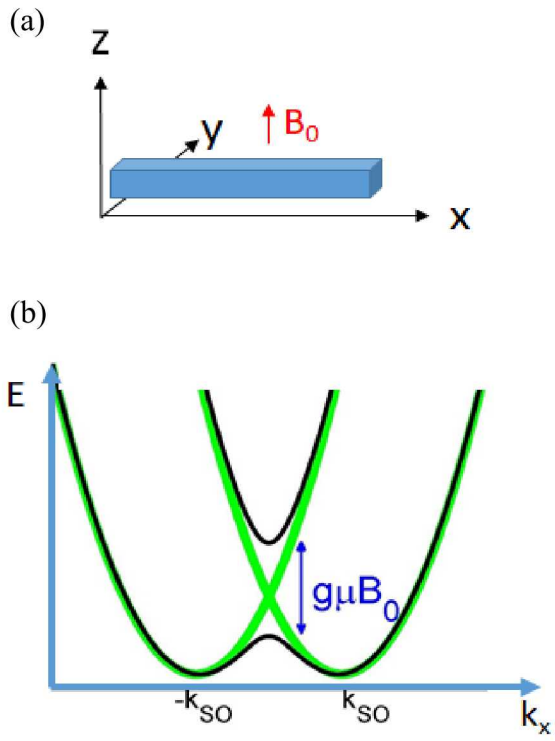

Fig. 1: (a) A spin-orbit coupled 1D system along the x-direction in the presence of an external magnetic field along the z-direction. (b) The associated band diagram. Without an external magnetic field, the dispersion is degenerate at $k_x = 0$. The external magnetic field opens up an energy gap in the spectrum, as shown by the black curves. Inside this spin-orbit gap, only two degenerate states exist at each energy, and they are spin-momentum locked.

Finding topological superconductors is an extremely challenging task in its own right. It was therefore a nice surprise when Fu and Kane showed in 2008 that one can obtain an effective topological superconductor by combining a conventional superconductor and a topological insulator [8]. Later, it was further shown that even conventional semiconductors, when in close contact with a conventional superconductor, can turn into topological superconductors as long as the spin-orbit coupling (SOC) is sufficiently strong [9-13]. Since the growth, processing, and physical properties of semiconductors are much more well understood than topological insulators, it seems natural to use such semiconductor/superconductor

hybrid systems as the starting point for the search of MZMs. Many experimental efforts have been put forth and much progress indeed has been made [14-18].

The configuration that is the easiest to understand and the most widely adopted experimentally is a one-dimensional (1D) semiconductor with strong intrinsic SOC, as shown in Fig. 1(a). The energy-momentum (E-k_x) dispersion relations of such a 1D system with and without the presence of a magnetic field perpendicular to the SOC-induced effective magnetic field are shown in Fig. 1(b) in black and green. At zero magnetic field, the dispersion is simply two identical parabolas shifted left and right from $k_x=0$, effected by the SOC which behaves as a k_x dependent magnetic field. The shift is characterized by k_{SO}, which is proportional to the SOC constant. In the presence of an external magnetic field that is perpendicular to the SOC-induced effective magnetic field, the two crossing branches near $k_x=0$ mix and anti-cross, opening up a spin-orbit gap near $k_x=0$ that is proportional to the external magnetic field and the effective g factor. Inside this energy gap, only two degenerate states exist at each energy. The spin and momentum are locked. When a conventional superconductor is in close electrical contact, an effective 1D topological superconductor forms and MZMs appears at the ends of the 1D system, if the Fermi energy is inside the gap and if the external magnetic field is sufficiently large. This is the precisely the setup used in the experiments that have produced the most convincing evidence of MZMs [14-18]. In those experiments, InAs or InSb nanowires were the chosen semiconductor materials for their small effective mass, large g factor, and, most importantly, intrinsically strong SOC.

While the evidence of MZMs in these InAs or InSb nanowire/superconductor hybrid systems has been accumulating and becoming more convincing, two natural questions to ask are how we can perform quantum operations on these MZMs and how we can scale up for more realistic quantum computation needs. One potential approach pursued by several leading groups is to continue the development of InAs and InSb nanowires. There the difficulty lies in the controlled growth/synthesis of two-dimensional arrays of uniform nanowire/superconductor heterostructures.

An alternative path, investigated in this Laboratory Directed Research and Development (LDRD) project, is to use a semiconductor that is more technologically mature in growth and material processing, and preferably compatible with modern semiconductor foundry processes. From this perspective, Si emerges as the most preferred semiconductor, as it is arguably the most well understood electronic material and the supporting infrastructure is simply unparalleled.

However, the intrinsic physical properties of electrons in Si are highly unfavorable for the pursuit of MZMs: the effective mass is large, the g factor is small, and, most importantly, the intrinsic SOC is extremely weak. While in 2012, it was shown by Kjaergaard et al. that MZMs can exist in a 1D semiconductor without SOC if a fine-pitch nano-magnet array is placed next to the wire and if superconductivity is induced [19], the calculation was done for InAs, a material with a smaller effective mass and a large g factor. No band structure was calculated, either. It was therefore unclear whether it is possible at all to create a sizable effective spin-orbit gap in Si.

Furthermore, very few studies of superconducting electrons in Si exist, making the feasibility of creating MZMs in Si highly uncertain.

In spite of the high risk, the potential payoff of a Si-based topological quantum computing platform nevertheless warrants a careful examination of the two questions. What we set out to investigate in this two-year LDRD project was mainly to address the first question: can one engineer the SOC in Si so that the very weakly spin-orbit coupled material effectively behaves as one with strong SOC? We also dabbed into the induced superconductivity through external collaborations.

The project was organized into four tasks.

1. Theoretical analysis, three-dimensional (3D) simulations of the magneto-statics, and spin-dependent band structure calculation.
2. Development of magnetic materials with controlled coercivity and magnetization.
3. Formation and programming of nano-magnet arrays with the required magnetization configuration.
4. Induced superconductivity in Si.

The results of each task will be described in more details in section 2. We provide a brief summary for each task here.

1. We have set up 3D models using COMSOL Multiphysics for magneto-static simulations that can generate the nanoscale magnetic field distribution resulting from nano-magnets included in the model. The nanoscale magnetic field distribution can then be fed into a spin-dependent Hamiltonian for band structure calculation. With an optimized, experimentally realizable nano-magnet configuration, an effective spin-orbit gap of ~0.3 K is indeed achievable. A manuscript summarizing this effort was submitted to Physical Review Applied in January 2018 and re-submitted in September 2018 after revision [20].
2. We have developed processes for depositing SmCo thin films with controlled coercivity. Systematic materials characterizations have led to a coherent understanding of the magnetic properties of SmCo thin films at the microscopic and macroscopic levels. A manuscript reporting our systematic investigation was submitted to Journal of Magnetism and Magnetic Materials in August 2018 [21].
3. By using SmCo, which has high coercivities, and Co, which has low coercivities, we successfully fabricated and programmed nano-magnet arrays with alternating magnetization directions, the required configuration for effecting the spin-orbit gap. A manuscript on this effort is in preparation.
4. Attempts to observe induced superconductivity in Si were made through external collaborations. We indeed observed signatures of induced superconductivity through the superconducting proximity effect but no supercurrents.

2. TECHNICAL RESULTS

2.1. Designing Nano-magnet Arrays for Topological Nanowires in Si

As described in Section 1, while ideas of using nano-magnets to engineer an effective SOC for creating MZMs in weakly spin-orbit coupled materials were proposed in 2012 [19], no band structure calculation based on realistic magnetic field distributions was presented. No numerical simulation result existed for Si-based systems. We have set up 3D models using COMSOL multiphysics to simulate the magneto-statics, which yield the nanoscale magnetic field distribution for a given nano-magnet configuration. The obtained magnetic field distribution is then plugged into a spin-dependent Hamiltonian using the material parameters for Si. The dispersion relation and the wave functions are obtained by numerically solving the Hamiltonian. Details of the mathematical analysis and numerical methods as well as the band structures, the design rules, and the feasibility analysis are all documented in our manuscript [20]. Here we only show the most important physical results. The understanding of the spin rotation in the presence of a spatially rotating magnetic field is not included in the manuscript and is therefore presented here.

2.1.1. Material platform

First, we argue that the best, and perhaps the only viable starting material platform is a shallow Si/SiGe quantum well [22].

As discussed in Section 1, the common starting point of the theoretical analysis for emergent MZMs in semiconductor nanowires is often a single-band, spin-orbit coupled dispersion. This assumption of an ideal dispersion relies on a clean and uniform semiconductor host material. A common metric for the cleanliness of the host material is mobility. In the case where the spin-orbit gap is created by nanomagnet arrays, as in the Si electron case, the mean free path (MFP) and phase coherence length are the more relevant metrics. A MFP and a phase coherence length that are larger than the spatial period of the nanomagnet arrays are desired. The phase coherence length diverges at zero temperature and can be much longer than the MFP at dilution refrigerator temperatures, so we consider here only the MFP. With our electron beam lithography (EBL) capability, nanomagnet periods in the range of 100 to 200 nm should be straightforward to achieve, and 50 to 100 nm feasible albeit demanding. The spatial period dictates where the zone boundaries are, and in turn, the electron density at which the chemical potential is inside the spin-orbit gap. Taking 100 nm as an estimate, the required 1D electron density would be 2/(100 nm). Since most available data on electron densities and mobilities are based on two-dimensional (2D) electron systems, for estimation purposes, we estimate the required 2D electron density to be $(2/(100\ \text{nm}))^2$, which is 4×10^{10} cm^{-2}. A nanomagnet period of 50 nm quadruples the required 2D density (1.6×10^{11} cm^{-2}). The required MFPs are 100 and 50 nm accordingly.

Such demanding requirements on low densities and long MFPs rule out conventional Si metal-oxide-semiconductor field-effect transistors (MOS FETs) as the host material for MZMs. Due to the close proximity to an amorphous SiO_2 layer, 2D electrons in Si

MOS FETs are typically insulating below ~8×10^{10} cm^{-2} with a resistivity ~ h/e^2 [23], which translates to a MFP less than 20 nm. At 1.6×10^{11} cm^{-2} with a typical mobility of 1×10^4 $cm^2V^{-1}s^{-1}$ in a MOS FET, the MFP is still less than 50 nm.

On the other hand, Si/SiGe quantum well heterostructures can support high-mobility electrons in Si quantum wells owing to the epitaxially smooth interfaces where the 2D carriers reside [24]. Mobilities exceeding 10^6 $cm^2V^{-1}s^{-1}$ have been demonstrated [25]. More importantly, very low carrier densities, in the range of 10^{10} cm^{-2}, are achievable using the SiGe heterostructure field-effect transistor (HFET) architecture [22]. We thus chose Si/SiGe quantum wells as the starting material.

2.1.2. Controlling Gaps and Design Advice

In the presence of a purely spatially rotating magnetic field, our simulation results show that an effective spin-orbit gap opens up. For realistic magnetic field distributions that result from nano-magnets, an additional feature shows up in the dispersion: tiny gaps open up in the two supposedly continuous branches as a result of non-ideal field distributions. While these tiny gaps (called bad gaps in our manuscript) do not completely destroy the topological superconductor and the emergence of MZMs, they shrink the operating window and enhance backscattering.

A careful Fourier analysis of the Hamiltonian gives us the following recipe for optimizing the gaps (maximizing the good spin-orbit gap and minimizing the bad gaps):

The magnetic field components should have their first Fourier coefficients 90 degrees out of phase, equal in magnitude, and be as large as possible.

2.1.3. Designs with Only One Magnet Polarization

In the original proposal by Kjaergaard et al., a design where all the magnets are polarized in the same direction was claimed to be a viable configuration [19]. However, our simulation results show that the magnetic field distributions resulting from such nano-magnet configurations have non-zero average magnetic fields, which introduce very large energy gaps. The effective spin-orbit gap is not identifiable in the dispersion.

Nontheless, an interesting layout strategy was identified by us that allows using nano-magnets polarized in the same direction. The key realization was that the local magnetic field due to a nano-magnet points opposite directions near the tips and near the waist. By strategically placing nano-magnets at precise locations, we showed that it is indeed possible to use only nano-magnets polarized along the same direction. The difficulty lies in the required high precision in nano-magnet placement, which may not be achievable experimentally.

2.1.4. Tower Magnets

We also realized that by standing the nano-magnets up so that the tips of them point directly at the 1D channel ensures the highest degree of proximity. Our simulation results show that a 0.3 K spin-orbit gap is achievable using realistic dimensions and materials parameters. A gap as large as 0.3 K is very reassuring, as temperatures as

low as 20 mK are routinely achieved in dilution refrigerators and single-digit mK temperatures are possible using adiabatic demagnetization refrigeration.

.

2.1.5. Measuring the Spin-orbit Gap

An important question is how many periods is required for the dispersion to start to look like our simulations results, which assume an infinitely long periodic 1D system. We calculated the energy-dependent transmission through a finite nano-magnet array using the KWANT software package[26]. We pleasantly discovered that as few as four unit cells are required for the effective spin-orbit gap structure to be detectable.

2.1.6. *Spin Rotation*

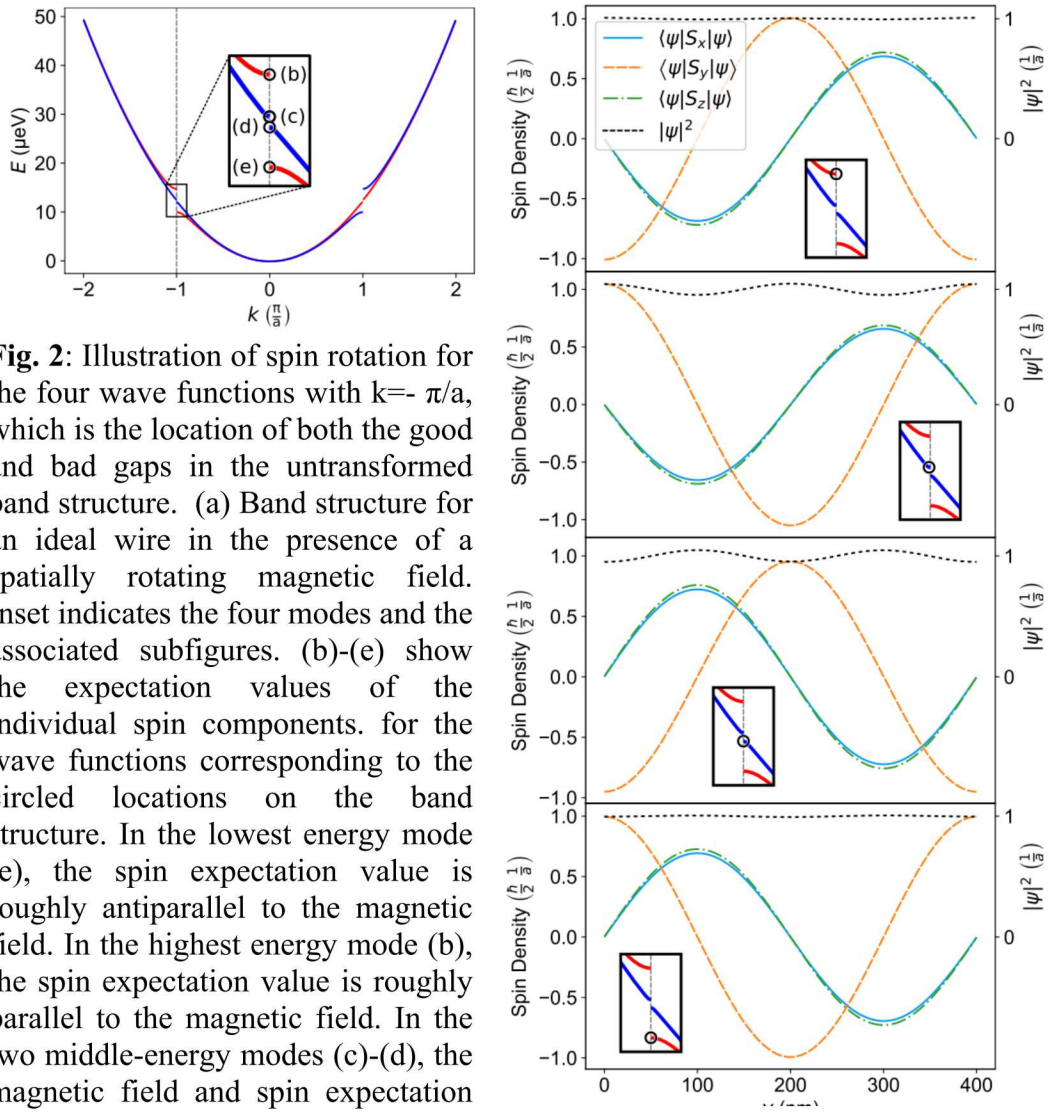

Fig. 2: Illustration of spin rotation for the four wave functions with k=- π/a, which is the location of both the good and bad gaps in the untransformed band structure. (a) Band structure for an ideal wire in the presence of a spatially rotating magnetic field. Inset indicates the four modes and the associated subfigures. (b)-(e) show the expectation values of the individual spin components. for the wave functions corresponding to the circled locations on the band structure. In the lowest energy mode (e), the spin expectation value is roughly antiparallel to the magnetic field. In the highest energy mode (b), the spin expectation value is roughly parallel to the magnetic field. In the two middle-energy modes (c)-(d), the magnetic field and spin expectation values rotate in opposite directions.

As this part will not be included in our manuscript [20], we provide more details. To understand the physics that causes the spin-orbit gap in the band structure, it is instructive to look at how an electron's spin rotates as it moves through the 1D channel. As an example, in Fig. 2 we illustrate the spin rotation in the states nearest the good and bad gaps at k=-π/a for an device in the presence of an ideal, spatially rotating magnetic field. The lowest energy state [Fig. 2(e)] has its spin roughly antiparallel to the spatially rotating magnetic field, while the highest energy state [Fig. 2(b)] has its spin roughly parallel to the spatially rotating magnetic field. In both cases, when viewed from the +z axis, the magnetic field and the spin expectation values rotate clockwise as we move along the +y axis. For the two states with intermediate energies [Fig. 2 (c) and (d)], the magnetic field and spin expectation

values rotate in opposite directions, so the energy shift is approximately zero. (If that were exactly zero, there would be no bad gap.) In all cases, the spin rotates with the same period as the magnetic field, and the magnitude of the wave function is fairly constant (black curve, right axis). These results are consistent with the simple physical picture that, when rotating spins are used as the basis, only the branches with the same chirality and period as the rotating magnetic field are strongly perturbed in energy. The rotation and wave function magnitude can be more complicated for other k values.

2.2. Tuning the Microstructural and Magnetic Properties of $SmCo_5$ Films

As described in Subsection 2.1, it is indeed possible to create an effective spin-orbit gap in the dispersion of electrons in Si (Si/SiGe quantum well heterostructures, to be more precise). The "help" for effecting the spin-orbit gap is nano-magnet arrays with controlled magnetization, both in direction and magnitude. While we discovered new designs that achieve the same goal do not require alternating magnetization directions, what we set out to explore was to find an experimentally viable approach to create nano-magnet arrays with alternating magnetization directions which, in turn, can generate the required spatially rotating magnetic field along a 1D channel.

There appears to be several paths for achieving this magnetic configuration. First, neighboring nano-magnets may exhibit an effective anti-ferromagnetic coupling to minimize the magneto-static energy. The desired magnetic configuration may simply result from de-magnetizing the nano-magnet arrays. The Second possibility is to program individual nano-magnets through some electrical or optical signals. This of course has the maximum flexibility and leads naturally to manipulation of MZMs should such modes indeed can be created this way. However, this is also the most difficult approach. Currently no technology exists for easily programming individual nano-magnets that have sizable magnetic moments. The last approach, chosen and pursued in our project, is to create two sets of interleaving nano-magnets. The essential component is to have the two sets of nano-magnets made out of two magnetic materials with distinct coercivities. The coercivity is, crudely speaking, the magnetic field required to flip the magnetization direction. By having two materials with distinct coercivities, we can use the following sequence of magnetic field sweeps to achieve global programming of the nano-magnets. First, a magnetic field higher than both coercivities is applied, aligning all of the nano-magnets to the same direction. The magnetic field direction is then subsequently reversed and the field is swept to a point between the two coercivites. The set of nano-magnets with the smaller coercivity now flips, while the other set retains the original orientation. The end result is a configuration with alternating magnetization directions.

The key to this global programming approach is the control of the coercivity of magnetic materials. The larger the contrast in coercivity, the larger the operating window and the higher the stability of the nano-magnets. To obtain a large contrast in coercivity implies the use of one soft magnetic material and one hard magnetic material. Further, the saturation magnetization of these materials should be as large as possible to maximize the size of the spin-orbit gap, which, based on the analysis

shown in the previous section, is proportional to the first Fourier component of the nanoscale magnetic field distribution.

The choice of the soft magnetic material is fairly straightforward: Co has a fairly high saturation magnetization (1.76 T, textbook value; ~2 T, measured by S. Eley) and has a small coercivity (~20 mT, measured by S. Eley). To choose a hard magnetic material, we considered two rare-earth magnetic alloys: SmCo and NdFeB. Both materials can have coercivities higher than 1 T and have ~1 T saturation magnetization. Attempts to sputter NdFeB failed in the early months of the project, while sputtering of SmCo films were straightforward, reliable, and repeatable. We thus focused on SmCo films in this project.

As-sputtered SmCo films are typically amorphous and have low coercivity. Post-growth annealing is required for hard magnetic phases, such as $SmCo_5$ crystallites, to form. We systematically performed a series of annealing experiments and characterized the annealed films through macroscopic analyses (x-ray diffraction (XRD)) and magnetic moment measurements), thin film characterizations (Rutherford backscattering and secondary ion mass spectroscopy), and microscopic imaing (atomic force microscopy, magnetic force microscopy (MFM), and transmission electron microscopy (TEM)). We obtained a comprehensive picture of how $SmCo_5$ thin films evolve structurally and magnetically upon annealing. The coercivity was shown to be fine controlled by the annealing temperature, and we were able to achieve a coercivity as high as ~1.5 T. The contrast in coercivity between annealed SmCo films and unanealed Co films is more than adequate for the fabrication of programming of nano-magnet arrays with alternating magnetization directions. These results have been documented in a manuscript submitted to Journal of Magnetism and Magnetic Materials [21]. Below is a summary of what we learned about controlling the properties of SmCo films.

The SmCo films we sputter are amorphous as deposited, as evidenced by TEM selected area electron diffraction. The coercivity is low (<0.1T). Upon anneal for 30 minutes at a given temperature in a close to ultra-high-vacuum environment (~10^{-7} torr), the magnetic properties of these films show little change when the annealing temperature T_{anneal}<=500 °C. However, when the films are annealed at T_{anneal}>500 °C, the coercivity rises, the saturation magnetization decreases, new peaks that can be identified as $SmCo_5$ appear in XRD, and TEM reveals nanocrystals embedded in a matrix. The coercivity continue to rise with the annealing temperature and reaches ~1.5 T at T_{anneal}=675 °C. Beyond this temperature, evidence of oxidation of the films appears in XRD. Concomitantly the coercivity drops sharply. There is thus an optimal window for annealing SmCo films.

MFM measurements yield estimates of magnetic moments consistent with macroscopic magnetization measurements. More importantly, MFM and magnetic moment measurements also reveal that the SmCo films exhibit perpendicular anisotropy (the preferred magnetization axis is perpendicular to the film) as deposited. Yet this perpendicular anisotropy weakens and eventually disappears when $SmCo_5$ crystallites form in the material. We tentatively ascribe the observed perpendicular anisotropy to bond-orientation anisotropy [27].

2.3. Forming and Programming Arrays of Nano-magnets

After we identified the two magnetic materials to use for forming we moved on to forming and programming nano-magnet arrays. An immediate task is was find a way to fabricate SmCo nano-magnets. EBL followed by lift-off is an apparent solution. Since our SmCo films are sputter-deposited and sputtering typically results in conformal coating, lift-off did not seem to be the best option. We thus attempted to form SmCo nano-magnets through an etch-back process. In parallel, we explored the feasibility of using lift-off to form SmCo nano-magnets. While the conformal coating indeed leads to undesirable "bat ears" on the nano-magnets as a result of tearing during the "lift-off" process, the nano-magnet patterns are robust enough to survive extensive sonication, which removes most of the "bat ears". By performing very-high-accuracy alignment, we were able to create the desired two sets of interleaving nano-magnets made out of SmCo (deposited first) and Co (deposited last). We achieve an alignment accuracy as good as 4 nm. By performing the programming sequence described in Subsection 2.2 and MFM imaging after each of the programming step, we successfully demonstrated the (global) programming of the nano-magnet arrays into alternating magnetization directions. A manuscript is being prepared for reporting these exciting results.

The results of our experiments on dry etching are documented here. We tested two dry etching methods, ion-milling and inductively coupled plasma - reactive ion (ICP-RIE) etching, to fabricate nano-magnets of SmCo5 alloy.

Ion milling is a mechanical etching process due to high-energy ion bombardment. Non-reactive gases, such as Ar, are used as the source of ions. The etching is obtained by the removal of surface atoms by sufficient momentum transfer from impinging ion to the surface atom. Ion milling is a highly anisotropic etching technique. Etching selectivity is poor by this technique compared to chemical methods as the etching rates mainly depend on the energy and mass of the incident ions, mass of the target atoms, and their surface binding energy. Plasma etching, on the other hand, is obtained by exposing the sample in the plasma generated in a chemically active gas environment in a low pressure chamber. In an ICP system, plasma discharge is obtained by electromagnetic induction. In a typical ICP-RIE etching process, chemical species react with the surface atoms or molecules and produce volatile byproducts which are removed in the process. The etching in ICP-RIE is further aided by the physical bombardment of the species (electrons, ions) in the plasma. High etch rates can be achieved using ICP-RIE, and the material selectivity can be high.

Dry etching of rare earth-transitional metal (RE-TM) alloys can be challenging due to the presence of heavy atoms in the alloy, strong chemical bonding, and weak reactivity [28]. Patterning of RE-TM nano-magnets can be further challenging if the etching selectivity of RE-TM alloy is not high enough compared to the mask used to define the pattern. We studied patterning of $SmCo_5$ nano-magnets by ion-milling and Cl-based ICP-RIE with different types of masks.

To obtain $SmCo_5$ nano-magnets by dry etching, line patterns were prepared on the SmCo films using standard EBL. In a typical procedure, negative or positive resist was spin coated depending upon the choice of the pattern mask, and then electron

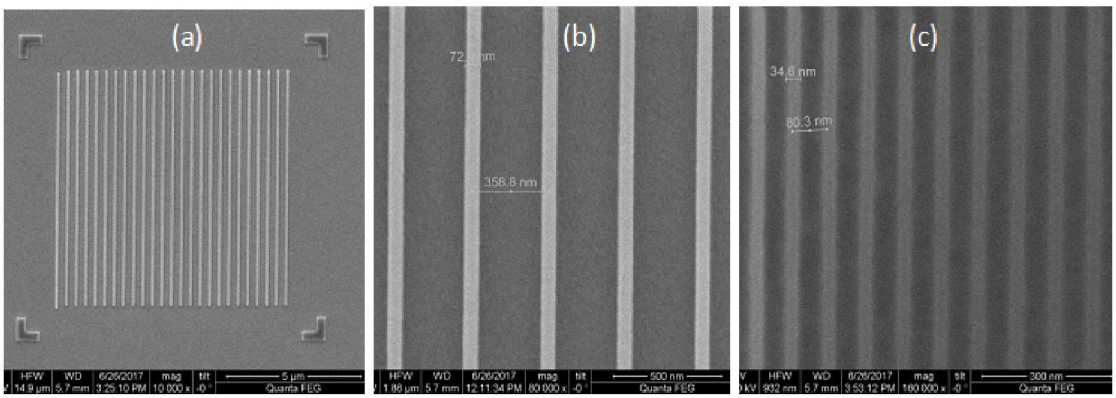

Fig. 3: SEM images of the HSQ line patterns on a SmCo film. (a) A block of line patterns. (b) 72 nm wide lines with a pitch of 358 nm. (c) 35 nm wide lines with a pitch of 80 nm.

beam was written on the resist. We used an scanning electron microscope (SEM) for the patterning. The patterns were developed in an appropriate developer solution; for negative resist hydrogen silsesquioxane (HSQ), tetramethylammonium hydroxide (TMAH) was used at 40 °C, and for positive resist poly-methyl methacrylate (PMMA), methyl isobutyl ketone (MIBK) was used by mixing it with isopropyl alcohol (IPA) (1 part MIBK:3 parts IPA). The prepared HSQ patterns were used as masks for etching without any further processing, whereas either Al_2O_3 or Cr were deposited on the PMMA patterns followed by lift off to form a hard mask for the dry etching step. Typically 10 μm long and 35 – 200 nm wide line patterns were fabricated, and the pitch of the lines was in the range of 80 nm to 500 nm. Figure 3 shows the HSQ line patterns prepared on a SmCo film.

bIon milling experiments were carried to etch SmCo samples patterned with HSQ lines. The HSQ patterns were ~80 nm thick. The milling was performed in the ion milling tool at CINT. In the milling process, sample was loaded in the ion milling chamber and pumped down to 3×10^{-7} Torr. Ar gas was supplied through the hot filament to produce Ar ions which were then accelerated to gain ~500 eV of energy. The ion flux of 1 mA/cm^2 was exposed on the HSQ patterned SmCo films for different etch times. The etched samples were then dipped into deionized water to remove residues. The etching depth of each the sample was measured using a stylus profilometer. The various etch times and the etching depths are tabulated below.

Table 1: Etching of SmCo5 films by ion milling with HSQ mask

Etching Time	**Etching Depth**	**Comments**
65 seconds	16 nm	Rounded edges, no significant damage
120 seconds	28 nm	Rounded edges, no significant damage

180 seconds	38 nm	Moderate damage of the patterns
240 seconds	52 nm	Significant damage of the patterns

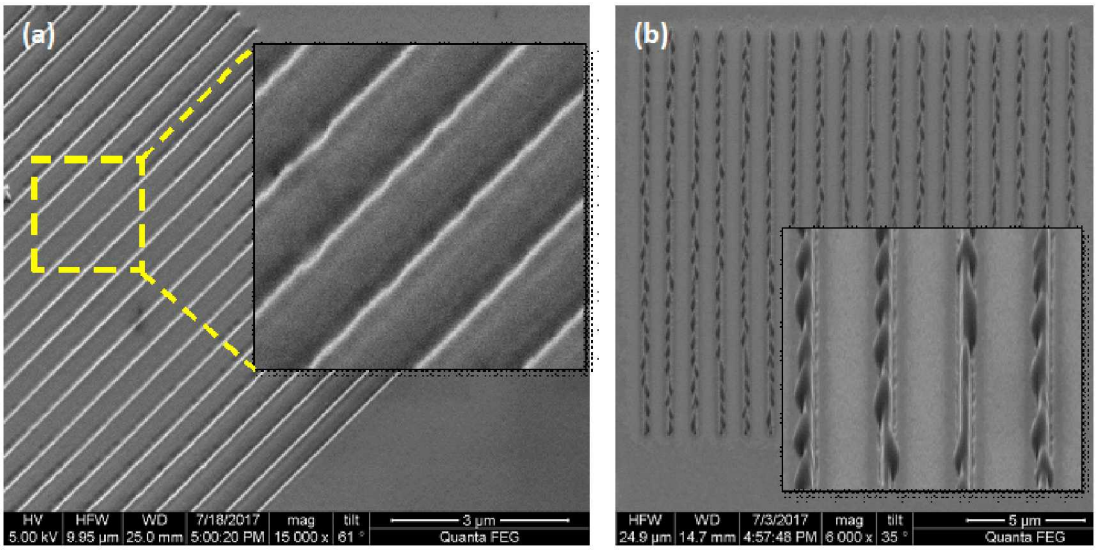

Fig. 4: SEM images of $SmCo_5$ nano-magnets patterns after ion milling for (a) 65 s and (b) 240 s. Insets are the magnified views. Significant pattern damage can be seen in (b).

Figure 4 shows the SEM images of the $SmCo_5$ patterns etched by ion milling. The etch rate was found to decrease for longer etching time. HSQ forms amorphous SiO_2 over soft bake and the ion milling selectivity of $SmCo_5$ to SiO_2 can be as high as 12 to 1 [28]. However, when the pattern sizes of HSQ are sufficiently small, the selectivity can be smaller as the lateral etching of the patterns can be significant. When the etching time is as long as 4 minutes, significant damage of the SmCo5 patterns was observed. We thus concluded that ion milling could not achieve the goal of this project to fabricate high-quality $SmCo_5$ nano-magnets.

It has been reported that mixing of Cl_2/Ar discharge enhances the etching rate by nearly 10 fold compared to pure Ar discharge [29]. The ICP-RIE etching was carried out in a CINT Trion ICP-RIE system. We experimented with both Cl_2/Ar and BCl_3/Ar based plasma, and found that the etch rate with Cl_2/Ar based plasma is nearly double of that of the BCl_3/Ar based plasma. ICP-RIE etching of $SmCo_5$ was tested with HSQ, Al_2O_3, and Cr masks. To prepare the Al_2O_3 or Cr mask patterns, EBL was performed on PMMA followed by thermal evaporation of Al_2O_3 or Cr and liftoff. Reasonable etching rate was obtained only when the RIE power was increased to more than 50W and the ICP power was set to more than 250 W. HSQ displayed an improved selectivity compared to the Ar ion milling but some damage and peeling off of the HSQ mask was observed. Etching selectivity of Al_2O_3 was also tested by covering part of a $SmCo_5$ film by an Al_2O_3 film without patterning it. While the Al_2O_3 film showed a selectivity of approximately 1 to 5 over the $SmCo_5$ film, patterned

Al_2O_3 masks completely disappeared after ICP RIE etching, as shown in Fig. 5. One explanation is that the deposited Al_2O_3 films were amorphous and were more sensitive to lateral etching. Cr displayed a similar etching rate as that of $SmCo_5$ but the $SmCo_5$ patterns obtained from Cr mask patterns were among the best, due to the least amount of damage. Table 2 summarizes the selected etch recipes used for $SmCo_5$ etching using HSQ, Al2O3 and Cr as the mask.

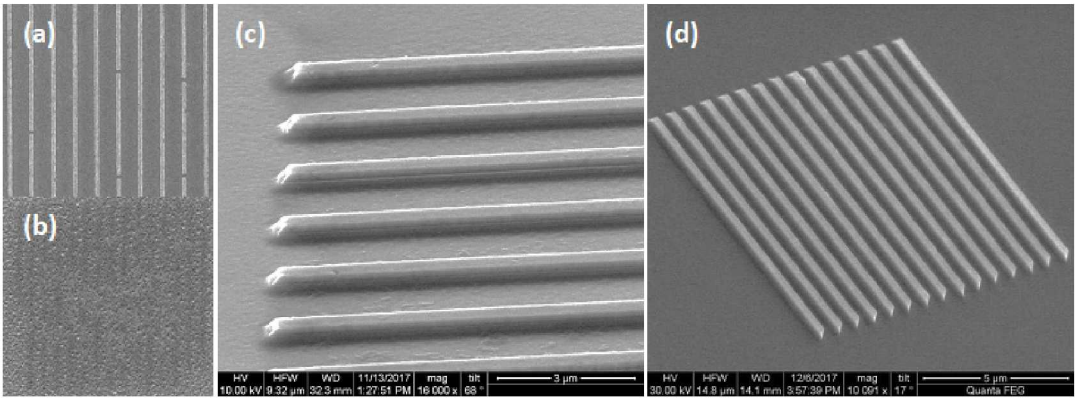

Fig. 5: Patterning of $SmCo_5$ by ICP-RIE. (a) Al_2O_3 patterns after lift-off. (b) Al_2O_3 patterns are completely removed by ICP-RIE. (c) $SmCo_5$ patterns obtained with an HSQ mask. (d) $SmCo_5$ patterns obtained with a Cr mask.

Patterning of $SmCo_5$ by dry etching is challenging due to the low etch rates and weak etching selectivity over the masking materials. The selectivity further reduces for smaller size mask patterns. We tested ion-milling and ICP-RIE etching using HSQ, Al_2O_3 and Cr as masks. We observed that ICP-RIE produced better results compared to ion milling by providing better selectivity and less damage on patterns. HSQ showed better etching selectivity among the three masks, however, some peeling of the HSQ patterns and damage of the $SmCo_5$ patterns were also observed. Cr has nearly 1 to 1 selectivity with $SmCo_5$ but we see the least damage to the patterns. Based on our results, we cannot recommend Al_2O_3 as a masking material for the etching of $SmCo_5$. HSQ is suitable for deeper etching, whereas Cr can be a suitable mask for shallower etching depths.

Table 2: ICP-RIE etching of the $SmCo_5$ films using various masks with selected recipes

Recipe	**Etch time**	**Etch depth**
P = 6 mT, ICP/RIE = 300/50W, BCl_3/Ar = 10/5 sccm	120 s	45 nm
P = 6 mT, ICP/RIE = 300/50W, Cl_2/Ar = 10/5 sccm	120 s	97 nm
*P = 10 mT, ICP/RIE = 300/70W, Cl_2/Ar = 20/10	100 s	52 nm

sccm		

2.4. Induced Superconductivity in Si

In the previous subsections, we have shown that a reasonably large spin-orbit gap in the energy spectrum of 1D electrons in Si is achievable with the help of nano-magnets and experimentally demonstrated the required magnetic configuration. The other essential component for observing MZMs is induced superconductivity. Surprisingly, there has not been much understanding of induced superconductivity in Si. There have only been a few reports on this topic in the past 30 decades, most of which concentrated in the 1980s. In particular, no reports existed on the superconducting proximity effect in Si/SiGe heterostructures. As our main focus was on the spin-orbit gap induced by nano-magnets, we collaborated with two external groups to address this question. We set up collaborations with Michel Pioro-Ladrière at Université de Sherbrooke and Javad Shabani at New York University.

Michel's group attempted to observe the superconducting proximity effect Nb/high-mobility 2D electrons/Nb devices where the high-mobility electrons are capacitively induced in a Si/SiGe quantum well structure. The devices were fabricated at CINT and shipped to Université de Sherbrooke for measurements. Signatures of the proximity effect were indeed observed in a device with 1um channel length. The zero-field small-bias resistance of the electron channel dropped by ~20% from 0.6 K to 0.2 K and then saturated. No supercurrent was observed. The results suggest that while there is indeed some induced superconductivity, the coherence length is much shorter than the channel length. The next logical step is to fabricated devices with much shorter channel lengths by EBL. The main complication is that PMMA, the most common EBL resist, may not survive the Nb deposition step. The temperature of the sample may rise so much that the thermal stress would cause the PMMA patterns to shift and break. This phenomenon, in fact, has been observed in other experiments.

Depositing superconductors on Si/SiGe structures is fairly straightforward, but the resulting interfaces are full of oxides, contaminations, defects, etc. These poor interfaces are known to suppress induced superconductivity and soften the superconducting gap. The preferred way of forming the superconductor/Si interface is epitaxial growth. The dilemma is that, in order to remove the oxides and contaminations at the starting Si surface, a high temperature anneal, as high as 900-1000°C under ultra high vacuum is typically required. SiGe heterostructures unfortunately do not survive at those temperatures. Strain relaxation and Ge diffusion are two main failure modes. Javad Shabani's group at New York University has set up an atomic hydrogen cleaning capability in an molecular beam epitaxy chamber. This capability allows the sample surface to be cleaned in situ at low temperatures so that the SiGe heterostructures can be preserved. We thus started a collaboration with his group to grow Al on Si/SiGe epitaxially and to see if a clean superconducting gap and supercurrent can be achieve. Their group will perform the device fabrication and low temperature measurements at New York University. Their molecular beam

epitaxy chamber has been properly set up for this experiment, device fabrication is in progress, and we expect to obtain preliminary measurement results in October 2018.

3. CONCLUSION

We set out to explore the feasibility of creating MZMs in a Si-based material platform. If successful, the results would pave the way to a practical topological quantum computing platform. There are two essential ingredients for creating MZMs in Si: (1) an effective spin-orbit gap in the energy spectrum of a 1D electron system and (2) induced superconductivity. We focused our resources on the former, and collaborated with two university groups on the latter.

Our theory and modeling results showed that an effective spin-orbit gap emerges in the energy spectrum of a 1D system if there is a nanoscale spatially rotating magnetic field. The size of the gap can be as large as 0.3 K, a temperature that is easily experimentally achievable, if the nano-magnets have an optimized layout. We also came up with designs that do not require nano-magnets with opposite polarities, albeit at the cost of more demanding fabrication.

Experimentally, we systematically investigate the effects of post-growth annealing on SmCo films. We found that the $SmCo_5$ crystallites form at annealing temperatures higher than 550 °C. This microstructural change is accompanied by a sharp increase in coercivity, which reaches ~1.5 T for films annealed at 675 °C. Beyond this annealing temperature, oxidation of SmCo occurs, probably because of residual oxygen in the chamber, and the coercivity drops. A process window was identified for tuning the coercivity of SmCo films. Through magnetic moment measurements and microscopic characterizations, we also found that the as-deposited SmCo films exhibit perpendicular anisotropy, a fairly unusual property for magnetic thin films. The perpendicular anisotropy appears to disappear around the same annealing temperature where SmCo crystallizes.

Combining the developed SmCo processes and electron beam evaporated Co, we successfully fabricated interleaving nano-magnets with an alignment accuracy as good as 4 nm. Exploiting the contrast in coercivity between annealed SmCo and unannealed Co, we programmed the nano-magnets into a configuration where the magnetization directions are alternating, as evidenced by MFM images. From both theoretical and experimental considerations, our results thus showed that it is indeed possible to create an effective spin-orbit gap in the spectrum of 1D electrons in Si.

We collaborated with two university groups to study the superconducting proximity effect in Si. The goal was to observe and characterize induced superconductivity in Si/SiGe heterostructures. Devices fabricated with electron beam deposited Nb showed some signatures of induced superconductivity but not supercurrent. Devices with epitaxial superconductor/Si interfaces are being fabricated and are expected to result in much improved superconducting properties.

At the program level, our results of this project have led many follow-on proposals. Two follow-on LDRD projects have been funded: "Nanomagnet-based physically unclonable functions," funded by the Exploratory Express Investment Area for fiscal year 2018 and "Magnetic Field Synthesis at the Nanoscale for Engineered Quantum Materials," funded by the Materials Science Research Foundation Investment Area for fiscal years 2019-2021. Another LDRD proposal "Superconducting Si" was selected for full proposal by the Advanced Science and Technology Investment Area but was not funded. A full proposal "Silicon-Nanostructure-Based Topological Quantum Systems" was submitted to the Basic Energy Science program at Department of Energy, Office of Science for the Department of Energy Early Career Awards. It was not selected for the Award, but the Basic Energy Science program is willing to consider funding a project on this topic.

REFERENCES

1. A. Steane. Quantum computing. Rep. Prog. Phys. 61, 117 (1998). doi: 10.1088/0034-4885/61/2/002

2. J. Clarke and F. K. Wilhelm. Superconducting quantum bits. Nature 453, 1031 (2008). doi: 10.1038/nature07128

3. C. Kloeffel and D. Loss. Prospects for spin-based quantum computing in quantum dots. Annu. Rev. Condens. Matter Phys. 4, 51 (2013). doi: 10.1146/annurev-conmatphys-030212-184248

4. F. A. Zwanenburg, A. S. Dzurak, A. Morello, M. Y. Simmons, L. C. L. Hollenberg, G. Klimeck, S. Rogge, S. N. Coppersmith, and M. A. Eriksson. Silicon quantum electronics. Rev. Mod. Phys. 85, 961 (2013). doi: 10.1103/RevModPhys.85.961

5. C. Nayak, S. H. Simon, A. Stern, M. Freedman, and S. Das Sarma. Non-Abelian anyons and topological quantum computation. Rev. Mod. Phys. 80, 1083 (2008). doi: 10.1103/RevModPhys.80.1083

6. A. Y. Kitaev. Unpaired Majorana fermions in quantum wires. Phys. Usp. 44, 131 (2001). doi: 10.1070/1063-7869/44/10S/S29

7. A. Y. Kitaev. Fault-tolerant quantum computation by anyons. Ann. Phys. (N.Y.) 303, 2 (2003). doi: 10.1016/S0003-4916(02)00018-0

8. L. Fu and C. L. Kane. Superconducting Proximity Effect and Majorana Fermions at the Surface of a Topological Insulator. Phys. Rev. Lett. 100, 096407 (2008). doi: 10.1103/PhysRevLett.100.096407

9. J. D. Sau, R. M. Lutchyn, S. Tewari, and S. D. Sarma. Generic New Platform for Topological Quantum Computation Using Semiconductor Heterostructures. Phys. Rev. Lett. 104, 040502 (2010). doi: 10.1103/PhysRevLett.104.040502

10. J. Alicea. Majorana fermions in a tunable semiconductor device. Phys. Rev. B 81, 125318 (2010). doi: 10.1103/PhysRevB.81.125318

11. R. M. Lutchyn, J. D. Sau, and S. D. Sarma. Majorana Fermions and a Topological Phase Transition in Semiconductor-Superconductor Heterostructures. Phys. Rev. Lett. 105, 077001 (2010). doi: 10.1103/PhysRevLett.105.077001

12. Y. Oreg, G. Refael, and F. von Oppen. Helical Liquids and Majorana Bound States in Quantum Wires. Phys. Rev. Lett. 105, 177002 (2010). doi: 10.1103/PhysRevLett.105.177002

13. J. Alicea. New directions in the pursuit of Majorana fermions in solid state systems. Rep. Prog. Phys. 75, 076501 (2012). doi: 10.1088/0034-4885/75/7/076501

14. V. Mourik, K. Zuo, S. M. Frolov, S. R. Plissard, E. P. A. M. Bakkers, and L. P. Kouwenhoven. Signatures of Majorana fermions in hybrid superconductor-semiconductor nanowire devices. Science 336, 1003 (2012). doi: 10.1126/science.1222360

15. L. P. Rokhinson, X. Liu, and J. K. Furdyna. The fractional ac Josephson effect in a semiconductor–superconductor nanowire as a signature of Majorana particles. Nat. Phys. 8, 795 (2012). doi: 10.1038/nphys2429

16. M. T. Deng, C. Yu, G. Huang, M. Larsson, P. Caroff, and H. Q. Xu. Anomalous Zero-Bias Conductance Peak in a Nb–InSb Nanowire–Nb Hybrid Device. Nano Lett. 12, 6414 (2012). doi: 10.1021/nl303758w

17. M. T. Deng, S. Vaitiekenas, E. B. Hansen, J. Danon, M. Leijnse, K. Flensberg, J. Nygård, P. Krogstrup, and C. M. Marcus. Majorana bound state in a coupled quantum-dot hybrid-nanowire system. Science 354, 1557 (2016). doi: 10.1126/science.aaf3961

18. S. M. Albrecht, A. P. Higginbotham, M. Madsen, F. Kuemmeth, T. S. Jespersen, J. Nygård, P. Krogstrup, and C. M. Marcus. Exponential Protection of Zero Modes in Majorana Islands. Nature 531, 206 (2016). doi: 10.1038/nature17162

19. M. Kjaergaard, K. Wölms, and K. Flensberg. Majorana fermions in superconducting nanowires without spin-orbit coupling. Phys. Rev. B 85, 020503 (2012). doi: 10.1103/PhysRevB.85.020503

20. L. N. Maurer, J. K. Gamble, L. Tracy, S. Eley, and T. M. Lu. Designing Nanomagnet Arrays for Topological Nanowires in Si. Submitted to Phys. Rev. Appl. Available on arXiv:1801.03676

21. K. R. Sapkota, S. Eley, E. Bussmann, C. T. Harris, and T. M. Lu. Tuning the Microstructural and Magnetic Properties of $SmCo_5$ Films. Submitted to J. Magn. Magn. Mater.

22. D. Laroche, S.-H. Huang, E. Nielsen, Y. Chuang, J.-Y. Li, C. W. Liu, and T. M. Lu. Scattering mechanisms in shallow undoped Si/SiGe quantum wells. AIP Adv. 5, 107106 (2015). doi: 10.1063/1.4933026

23. B. Spivak, S. V. Kravchenko, S. A. Kivelson, and X. P. A. Gao. Colloquium: Transport in strongly correlated two dimensional electron fluids. Rev. Mod. Phys. 82, 1743 (2010). doi: 10.1103/RevModPhys.82.1743

24. F. Schaffler. High-mobility Si and Ge structures. Semicond. Sci. Technol. 12, 1515 (1997). doi: 10.1088/0268-1242/12/12/001

25. T. M. Lu, D. C. Tsui, C.-H. Lee, and C. W. Liu. Observation of two-dimensional electron gas in a Si quantum well with mobility of 1.6×10^6 cm^2/Vs. Appl. Phys. Lett. 94, 182102 (2009). doi: 10.1063/1.3127516

26. C. W. Groth, M. Wimmer, A. R. Akhmerov, and X. Waintal. Kwant: a software package for quantum transport. New J. Phys. 16, 063065 (2014). doi: 10.1088/1367-2630/16/6/063065

27. Y. Suzuki, S. Takayama, F. Kirino, N. Ohta. Single ion model for perpendicular magnetic anisotropy in re-tm amorphous films. IEEE Trans. Magn. 23, 2275 (1987). doi:10.1109/TMAG.1987.1065290.

28. J. J. Wang, J. R. Childress, S. J. Pearton, F. Sharifi, K. H. Dahmen, E. S. Gillman, F. J. Cadieu, R. Rani, X. R. Qian, and L. Chen. Dry Etch Patterning of $LaCaMnO_3$ and SmCo Thin Films. J. Electrochem. Soc. 145, 164 (1998). doi: 10.1149/1.1838670
29. A. Walther, C. Marcoux, B. Desloges, R. Grechishkin, D. Givord, and N. M. Dempsey. Micro-patterning of NdFeB and SmCo magnet films for integration into micro-electro-mechanical-systems. J. Magn. Magn. Mater. 321, 590 (2009). doi: 10.1016/j.jmmm.2008.09.028

DISTRIBUTION

1	MS1314	Tzu-Ming Lu	1867
1	MS1415	Art Fischer	1867
1	MS0665	Hy Tran	9100
1	MS1411	Rick Muller	1864
1	MS0665	Jeff Nelson	1421
1	MS0899	Technical Library	9536 (electronic copy)
1	MS0359	D. Chavez, LDRD Office	1911

Sandia National Laboratories